

TITLE OF DISSERTATION GOES HERE

Laurel Farris

20 August 2017

Committee:

Dr. R. T. James McAteer  
Dr. Jason Jackiewicz  
Dr. Nancy Chanover  
Dr. Laura Boucheron

Abstract

Abstract text will go here.

## CONTENTS

Introduction	1
The solar chromosphere	5
Magnetic field, structure, and the <i>plasma-β</i>	6
Challenges in observing the chromosphere	7
3-minute oscillations	8
History of 3mOs	8
Observations of 3mOs	9
Intensity vs Velocity	9
Location in chromosphere: (x/y)	9
Location in chromosphere: height (z)	9
Physical mechanism that generates the 3mOs	9
Slow, propagating magnetoacoustic waves from the photosphere	11
Natural response of chromosphere at the acoustic cutoff frequency	12
The flaring chromosphere	14
Flare emission and evolution	14
The Solar Dynamics Observatory (SDO)	19
The Atmospheric Imaging Assembly (AIA)	19
The Helioseismic and Magnetic Imager (HMI)	19
Enhanced chromospheric 3-minute oscillatory power associated with the 2011-February-15 X2.2 flare	21
Introduction	21
Observations and data reduction	21
Analysis	26
Results and discussion	26
Appendix: Physics background	35
Waves	35
The acoustic cutoff frequency	36
Derivation of the cutoff frequency	38
Coronal seismology	40
Kink waves	41

## INTRODUCTION

*“Overview” from proposal:*

Embedded in the main lightcurve of a solar flare are low amplitude, high frequency oscillations called quasi-periodic pulsations (QPPs). The chromosphere persistently oscillates at its acoustic cutoff frequency of 3 minutes, in both quiet and active regions. A recent study of QPPs revealed an enhancement in the 3-minute oscillatory power in thermal emission during the main phase of a flare ([Milligan et al. 2017](#)). Here I propose to probe the oscillatory response of the chromosphere to flares in greater detail by addressing the following science questions:

1. In which part(s) of the active region does the enhancement of the 3-minute power occur? Is it global or local?
2. When does the enhancement of the 3-minute power occur, relative to the phases of flare development and evolution? At what rate does the oscillatory power increase, and how long does the enhancement last?
3. How do chromospheric oscillations in velocity compare to oscillations in intensity during flares?
4. Do flares of different sizes show the same oscillatory behavior in the chromosphere?

The current hypothesis is that the oscillations reflect the natural response of the chromosphere to a disturbance, rather than a reflection of the periodicity of the disturbance itself. The questions above will be addressed by a dissertation project, to be carried out in three phases:

1. **Reproduce and augment the results from [Milligan et al. \(2017\)](#) by studying the spatial and temporal localization of the 3-minute power during the 2011 February 15 flare.** Data from the Helioseismic and Magnetic Imager (HMI) and from the Atmospheric Imaging Assembly (AIA), two instruments on board the *Solar Dynamics Observatory (SDO)*, will be analyzed, using the techniques of Fast Fourier Transforms (FFTs) and wavelet analysis. The preliminary results will then be expanded by isolating distinct components of the active regions to constrain the spatial variation and extent of the oscillatory response. Finally, a longer data set will be used to include time before and after the flare.
2. **Expand the methodology to include analysis of spectroscopic data from the *Interface Region Imaging Spectrograph (IRIS)*.** The spatial and spectroscopic capabilities of *IRIS* were designed to probe the chromosphere and transition region and address questions similar to those put forth here. Previous studies have found chromospheric oscillations to be more prominent

in velocity than in intensity, and the inclusion of spectroscopic data from *IRIS* in Phase II will benefit this study by removing some of the ambiguities present in intensity images (such as those with multiple spectral lines in a single bandpass), and providing information from multiple heights in the lower atmosphere.

3. **Apply the techniques from the previous two phases to multiple flares with a range of sizes.** The methodology developed in Phases I and II will be used to study multiple flares of various sizes in Phase III. The primary goal of this phase is to go beyond analysis of a single event and create a more general contribution to the flare model as a whole.

*single\_page\_freewriting.gdoc*

Copied from proposal, probably needs some revising. date?

The overarching theme of my research is the investigation of the role of the chromosphere in flares. The field of solar physics and space weather is unique in that it has a direct impact on humans and our way of life.

1. How does understanding details of the flare process help with space weather prediction?
  2. What is some common work done to contribute to learning about flares?  
Most work has focused on the corona
  3. Importance of chrom in general (maybe... seems like this just ends up being a bullet underneath flares...)
- Importance of chromosphere's role in flares:
    - Light we see is emitted from this layer
    - Why are there gaps? Chromosphere can be hard to study...

From current paper (09 October 2018): Flare dynamics can be probed via quasi-periodic pulsations (QPPs), low-amplitude variations that have been observed in flare emission during all phases and across all wavelength regimes, with periods between 1 and 10 minutes. The cause of long-period ( $\gtrsim 1$  minute) QPPs is generally thought to be one of two possible mechanisms. One is that they reflect the periodic buildup and release of magnetic energy through cycles of magnetic reconnection. The other is that they are triggered externally by the surrounding plasma. Many studies of QPPs have concentrated on non-thermal emission, but there are few reports of QPPs in thermal emission from the chromosphere associated with flares. date?

Flare emission contains QPPs, small scale oscillations within the main light curve. Most flare studies have been of non-thermal emission at the extreme ends of the spectrum (radio & x-ray). Chromospheric oscillations are revealed in thermal emission, of which not many studies have been carried out. A recent study of a solar flare (Milligan et al. 2017) revealed an enhancement of the 3-minute oscillatory power in thermal emission from the chromosphere, but not in x-ray emission. This indicates that the 3mOs were not excited according to the rate of energy injection, but rather that this was a response of the chromosphere at its own natural frequency, or cutoff frequency.

1. Motivation:

- “Few reports of QPPs in thermal emission in response to flare energization”.
  - 3mOs do not depend on rate of energy injection, but may transport a significant amount of mechanical energy, which needs to be included in the flare energy budget.
2. Methods:
- Lyman alpha emission
  - X-rays
  - AIA 1600, 1700
3. Main results/conclusions:
- 3m Enhancement in thermal emission, but not X-rays  
→ Not signature of flare energy, but natural response of chromosphere
  - Flare injected energy, causing chromosphere to oscillate at the cutoff frequency

For my project, I will probe the spatial dependence and temporal patterns of the oscillatory behavior of the chromosphere, using both images and spectra. I will then apply the developed methodology to multiple flares to compare results for flares of various sizes, contributing to the general field of solar flares and space weather prediction.

**From Monsue2016:** “... $\text{H}\alpha$  observations of chromospheric oscillations in the p-mode band can provide information about the physical processes occurring in flaring regions. In particular, **variations in the oscillatory power as a function of frequency, spatial position, and time can be used to probe energy transport at different heights within a flare.**” (emphasis added). *Thu Oct 18 16:11:32 EDT 2018*

## THE SOLAR CHROMOSPHERE

Response of chromosphere during flares: Most focus is on corona, where energy is stored and MR and CMEs are released. But chromosphere dominates the radiative energy budget, so somehow energy is transported down rapidly, and how the layers respond can help us characterize energy transport and conversion. *Written on the back of post-it notes pad, no date. Not sure if I was working on how to word something in paper/dissertation, or just testing myself to see if I know the point of my own research. 8/14/18*

To study the chromospheric response to flares, it is necessary to first understand the structure and dynamics of the chromosphere during quiet, non-flaring periods.

The chromosphere got its name from Lockyer and Frankland because of the vivid red color of the limb (from H $\alpha$  emission) before and after eclipses. According to Hudson (2007), the chromosphere is a “well-defined layer”.

Globally, the chromosphere is a complex, dynamic interface that lies between the visible disk of the photosphere and the hot corona. About 500 km above the base of the photosphere at  $\sim$ 5800 K, the temperature decreases with distance as one would expect from basic physics, until it reaches  $\sim$ 4200 K. This is known as the temperature minimum  $T_{min}$ , and marks the lower boundary of the chromosphere. The absolute thickness of the chromosphere varies in the literature, usually between 2000 and 5000 km (close to the radius of the Earth).

At the upper boundary of the chromosphere, the temperature rapidly increases to the order of a million K in the corona. This temperature jump takes place in a region defined as the transition region (TR), a relatively thin layer of plasma that separates the chromosphere from the overlying corona.

The base of the photosphere ( $z=0$ ) is defined as where  $\tau_{5000} = 1$ . The temperature reaches 10000 K at  $z \approx 2300$  km, and then skyrockets to a million K over the TR (Kneer & Von Uexküll).

*What makes the chromosphere a distinct, separate layer of the solar atmosphere? It can be defined in multiple ways, including temperature profile (Tmin to rapid increase that defines the TR), structure (high to low  $\beta$ ), or if you want to be really technical, the optical depth at the limb. Why is the atmosphere divided this way? What makes the chromosphere distinct from the other layers? date?*

The flaring chromosphere

## Magnetic field, structure, and the *plasma*- $\beta$

The lower region of the chromosphere reveals a magnetic network similar to that of the photosphere, up to  $\sim$ 1300-1500 km. The pattern reflects that of the supergranular pattern at the photosphere. Above this, the consistent, homogeneous plasma gives way to complex structures (see [Judge \(2006\)](#) for a review). At the boundary between these two regions, the dominant pressure changes from thermal gas pressure to magnetic pressure. This property is quantified in a parameter called the *plasma*  $\beta$ , defined as the ratio of thermal gas pressure to magnetic pressure:

$$\beta = \frac{P_{\text{thermal}}}{P_{\text{magnetic}}} = \frac{\rho k_B T / \mu m_{\text{amu}}}{B^2 / 8\pi} \propto \frac{\rho T}{B^2} \quad (1)$$

where  $k_B = 1.38 \times 10^{-16}$  [erg K $^{-1}$ ] is Boltzmann's constant,  $\mu$  is the average mass per particle in atomic mass units [amu],  $m_{\text{amu}} = 1.67 \times 10^{-24}$  [g] is the nucleon mass,  $\rho$  is the mass density,  $T$  is the local temperature, and  $B$  is the magnetic field strength [gauss].

In practice, a plasma is described by expressing its  $\beta$  relative to unity (rather than a specific numerical value). A plasma with  $\beta \gg 1$  is dominated by thermal pressure, and appears as a fairly homogeneous, uniform distribution of material. A plasma with  $\beta \ll 1$  is dominated by magnetic pressure and is characterized by complex structures, such as spicules and coronal loops. Figure

[reffig:plasma\\_beta](#) shows how  $\beta$  varies with height throughout the solar atmosphere. The balance between the two pressures plays a vital role in the structure and dynamics of a plasma, rather than the absolute strength of the magnetic field alone. At the  $\beta = 1$  boundary, mode conversion can occur for propagating acoustic waves.

Physics sidebar: mode conversion,  $\beta = 1$  surface.

Magnetic flux is generally concentrated in active regions, such as the umbrae of sunspots. As this flux rises into the atmosphere, it gives rise to the complex structures that are observed as the emission from particles that flow along magnetic field lines (a result of the so-called "frozen-in" theorem). Magnetic structures play an important role in diagnosing conditions in the solar atmosphere. Field lines often serve as waveguides for oscillations in the atmosphere, revealed indirectly by the manner in which the plasma responds to a disturbance. Structures are also a potential means of transportation of mass and energy to the corona.

The upper part of the chromosphere contains structures called spicules that emit the distinct, dark pink color of H $\alpha$ , and can be seen around the disk of the sun during solar

eclipses. Above the base of the photosphere (where  $T \approx 5800$  K), the temperature falls off with distance until it reaches the so-called *temperature minimum*, at  $T_{min} \approx 4200$  K. The height at which  $T = T_{min}$  marks the lower boundary of the chromosphere, about 500 km above the base of the photosphere. This is where acoustic waves shock and dissipate, causing a sharp increase in temperature. The absolute thickness of the chromosphere varies roughly between 2000 and 5000 km, slightly less than the radius of the Earth. The temperature reaches  $\sim 10000$  K at the upper boundary of the chromosphere, at  $z \approx 2300$  km, and then rapidly increases to  $T \gtrsim 10^6$  K in the corona. This temperature jump takes place in a region defined as the *transition region* (TR), a relatively thin layer of plasma that separates the chromosphere from the overlying corona. The temperature gradient in the solar atmosphere above the base of the photosphere is shown in Figure reffig:solar\_atm.

### Challenges in observing the chromosphere

Here are some challenges.

## 3-MINUTE OSCILLATIONS

### History of 3mOs

When were 3mOs first observed and why? What was the motivation behind the research article that produced the first results? date?

3mOs were first discovered via velocity observations in the quiet chromosphere ([Jensen & Orrall 1963](#)).

Intensity oscillations with periods of 2-3 minutes have been observed in the chromosphere starting in the 1960s. They have been observed via intensity variations in EUV lines. In active regions, intensity oscillations were discovered by [Beckers & Tallant \(1969\)](#) above sunspot umbrae in Ca<sup>+</sup>, and given the term “umbral flashes” to characterize both their location and transient nature. A short follow-up study from [Wittmann \(1969\)](#) revealed flashes with a period of 150 seconds (2.5 minutes). Beckers and company continued to pursue these oscillations in ([Beckers & Schultz 1972](#)), with more intensity oscillations and the addition of velocity measurements of the umbrae at the photospheric level. The highest power tended toward the area directly above sunspot umbrae, with peak-to-peak velocities up to 1 km s<sup>-1</sup>. They found clear periods of 178 seconds (2.97 minutes) at the umbral center, 255 seconds (4.25 minutes) at the umbral edge, and 300 seconds (5 minutes) in the penumbra. They did not find a connection between velocity oscillations in the photosphere and intensity oscillations in the chromosphere.

In the quiet chromospheric internetwork regions, the Fourier velocity power spectrum peaks at  $\sim$ 5.5 mHz (3 minutes) ([Orrall 1966](#)).

[Giovanelli \(1972\)](#) reported umbral oscillations in both velocity and intensity.

Many authors have dedicated multiple publications to investigating this phenomenon. Lites is the first author on many papers submitted over the course of a decade or so, between 1982 and 1992.

### Initial Interpretation

3mOs were initially believed to exist in cavities as trapped, standing waves ([Scheuer & Thomas 1981](#)). Chromospheric cavity between T<sub>min</sub> and TR ([Chae & Goode \(2015\)](#) → Leibacher & Stein (1981))

## Observations of 3mOs

### *Intensity vs Velocity*

*Location in chromosphere: (x/y)*

*Network/Internetwork*

*Active Regions*

*Umbra*

*Penumbra*

*Location in chromosphere: height (z)*

### **Physical mechanism that generates the 3mOs**

Both the origin of the 3-minute oscillations and the reason for their persistence remain unclear.

3mOs are currently interpreted as slow magnetoacoustic waves propagating along magnetic field lines.

Results from [Tian et al. \(2014\)](#) supported the propagation of shock waves with peak-to-peak velocity amplitude between 5 and 10 km s<sup>-1</sup>,  $\lesssim$  the local sound speed.

Many other authors have contributed to the current interpretation as slow propagating SMA waves. Similar results were found by [Brynnildsen et al. \(2004\)](#); [Maltby et al. \(1999\)](#); [De Moortel et al. \(2000\)](#)

- The periodic pattern of sharp blueshifts followed by gradual redshifts in velocity observations reveal a sawtooth shape characteristic of propagating shock wave fronts.
- The shift toward the blue wing in emission lines (toward the observer) indicates that indicates an upward propagation through the atmosphere. The lack of accompanying redshift supports the interpretation of propagating waves and not standing waves reflected back toward the solar surface.

The previous two points (blueshift and sawtooth pattern) have lead to the interpretation of these patterns as manifestations of upward propagating magnetoacoustic waves along magnetic field lines.

Bogdan & Judge (2006), page 319: Various ionization stages (increasing T) → high space and time coherence at different heights in the 3-min band. High time cadence → phase shifts, which agree with wavepackets propagating from photosphere to the base of the chromosphere with vertical phase velocity  $\sim c_s$  (7-12 km per second).

### What is the manner in which oscillations propagate from the photosphere to the chromosphere?

The photosphere was already known to oscillate at a dominant frequency of 5 minutes. 5-minute oscillations are observed in the chromosphere as well, mostly in the network regions of the quiet sun, where magnetic field strength is relatively high. 3mOs are possibly connected to the global 5-minute oscillations.

The 5-minute period in the photosphere has been attributed to the global pulsations of the sun due to pressure modes (p-modes) in the interior. In the photosphere, the Fourier power spectrum peaks at  $\sim 3$  mHz (5 minutes) in the quiet sun. This power is reduced by a factor of 2-5 at the umbra of sunspots, though it is still the dominant frequency (?). The amplitudes of intensity variations in the photosphere tend to be relatively small and difficult to measure, while those in the chromosphere are dominated by the aforementioned umbral flashes. The non-isothermal region where a compressive acoustic disturbance is propagating along the magnetic field in direction  $\hat{k}$  Umbral  $\vec{B}$  aligned with  $\vec{g}$ , so  $H_{||} \rightarrow$  ‘true’  $H_P$ .

$$k_{||}^2 = \frac{\omega^2}{c^2} - \frac{1}{4H_{||}^2} \quad (2)$$

where  $\omega = 2\pi\nu$  and  $H = H_P$ , the pressure scale height (Cally 2001; Crouch & Cally 2003).

Waves propagate if  $k_{||}^2 \geq 0$  ( $\omega \geq c/2H_{||}$ ) threshold = acoustic cutoff frequency.  $\Omega = \Omega(z) = \max$  value of 5.2 - 5.5 mHz (3.21 - 3.03 minutes) with  $T_{\min}$  [Figure 2. of Cally et al. 1994 date?](#) 3-minute oscillations at the high frequency tail of photospheric oscillations. Conservation of wave energy: amplitude of velocity oscillation  $\propto 1/\sqrt{\rho}$  for waves with frequency greater than the cutoff. For waves with frequency less than the cutoff, “osc do not give rise to prop. waves”. Dispersion relation determines decline in velocity predicted by the imaginary part of the wave number.

“The dominant power above SS umbrae changes from 5 minutes in the photosphere to 3 minutes in the chromosphere because of strong spatial damping of evanescent waves with height, whereas 3mOs at the cutoff frequency are not damped.” [Milligan et al. \(2017\) → Noyes & Leighton 1963. date?](#) Vertical velocity oscillations extending into the chromosphere (Judge (2006) → Jensen & Orrall (1963); Noyes & Leighton (1963)).

## What is the manner in which oscillations propagate from the chromosphere to the corona?

Bogdan & Judge (2006) [and Tian et al. \(2014\)? date?](#) : Intensity oscillations (in emission lines) have been observed to “disappear” after traveling from the chromosphere through the transition region toward the corona (around  $T \geq 10^6$  K). The disappearance of a wave is generally attributed to dissipation, damping, or mode conversion. Thermal conduction is the principal dissipation mechanism at coronal temperatures, but it doesn’t affect 3mOs until they travel a few thousand km into the corona. Slow magnetoacoustic waves are not subject to Ohmic dissipation. Viscosity can be neglected for a collisionless plasma. They canāŽt be converted from slow to fast magnetoacoustic waves because this phenomenon would take place at the coupling region (where  $\beta \approx 1$ ), and the waves are observed to propagate at heights well above this. This observation also cannot be explained by reflection at some layer because that would result in a redshift in the observations, which is not the case. The best explanation is that the rapid increase in the temperature scale height causes the waves to dissipate.

$$\frac{2\pi}{k_{||}} \gg H_T \quad (3)$$

A wavetrain passing through the formation height of line causes uniform lift, compression, descent, and rarefaction over the entire layer over a single wave period. Exception to this: strong resonance lines like Ca II H & K and H $\alpha$ , which are optically thick and broad. Coronal emission lines are optically thin.

Compression and rarefaction reduce the overall contributions to net fluctuations in coronal emission line. Fe XVI: Changes in emission line intensity time series as move upward in z (and hence, in T) [OShea et al. \(2002\) date?](#) How high do they propagate? This question was posed by Reznikova et al. (2012).

There are two dominating theories of where the 3mOs originate.

### *Slow, propagating magnetoacoustic waves from the photosphere*

One is that they are generated below the chromosphere and propagate upward. The dominant peak at 3 minutes is explained by the acoustic cutoff frequency in the chromosphere, which is around 5.5 mHz. [See appendix or sidebar for physics details on the cutoff frequency? This is where my own plot should go! date?](#) Waves with frequencies lower than the cutoff are unable to continue propagating, therefore lower frequencies

(longer periods) are not observed at those heights. [What heights? Where does  \$\omega\_0\$  reach a maximum? date?](#)

### *Natural response of chromosphere at the acoustic cutoff frequency*

The second theory regarding the origination of 3-minute oscillations is that the acoustic cutoff frequency is the frequency at which the chromosphere naturally responds when a disturbance is introduced. In other words, the oscillations are generated within the chromospheric plasma, where they are observed.

This theory has been investigated and predicted by several authors. [Fleck & Schmitz \(1991\)](#) found similar behavior in both isothermal and non-isothermal models, suggesting that the temperature gradient throughout the chromosphere does not have an effect on its oscillatory response. [Kalkofen \(1994\)](#) simulated disturbances from both a single impulse and a continuous jostling (i.e. a periodic piston), with frequencies above and below the cutoff. The response to the single pulse tended toward the cutoff value, analogous to a bell sounding at a particular frequency when it is struck. A series of papers analytically examined adiabatic wave excitations in a gravitationally stratified atmosphere ([Sutmann & Ulmschneider 1995a,b](#); [Sutmann et al. 1998](#)). These studies also supported a similar response to a disturbance, regardless of whether they were impulsively or continuously introduced into the atmosphere. [Chae & Goode \(2015\)](#) used simulations of a gravitationally stratified medium to show that 3-minute oscillations naturally arise when such a medium is disturbed.

While many studies have predicted this behavior, actual observations of this phenomenon are quite rare. [Kwak et al. \(2016\)](#) observed enhanced oscillations in response to a downflow event attributed to a plume-like feature above the umbra of a sunspot.

#### Physics sidebar: **What are slow magnetoacoustic waves?**

Like standard acoustic waves, magnetoacoustic waves are longitudinal, compressible, and anisotropic waves in a magnetized plasma. They perturb the plasma density, allowing intensity variations to be observed. They also perturb the parallel component of the magnetic field [or velocity? date?](#). MA waves exist as either slow or fast MA waves, both of which can be either standing or propagating. Slow magnetoacoustic waves tend to damp out quickly (after 1-3 oscillations) due to energy losses from radiation/thermal conduction. They travel sub-sonically; their speed (phase velocity) is lower than the local sound speed. They are polarized perpendicular to the magnetic field. They are observed [at least in the corona date?](#) via both intensity variations (in EUV lines) and Doppler shifts. (See [Nakariakov](#)

& Verwichte (2005) for a general review of MHD waves and coronal seismology). Speed close to sound speed allows interpretation of slow, propagating MA waves.

## THE FLARING CHROMOSPHERE

What was originally observed by people (which takes place in history long before we observed the different wavelength regimes and started to understand the physical mechanisms giving rise to them). *Mon Feb 25 03:58:44 MST 2019*

[Sun Nov 18 18:17:21 MST 2018 date?](#) Do charged particles travel along magnetic field lines via the Lorentz force? Is particle beam composed of both electrons and ions, or just electrons? Are ions only visible in gamma rays? Do they hit the chromosphere?

*Rocket analogy*

The episodic, rapid release of magnetic energy in the solar atmosphere associated with flares, CMEs, and SEP events has the potential to wipe us out. Thus the field of space weather emerged and is devoted to understanding and preparing for these events. Much like a rocket booster, this outward burst of energy needs something to push against, and the same acceleration occurs in the opposite direction: down toward the lower layers of the atmosphere. Most research has focused on the rocket: the energy and material released outward into space. However, it is impossible to understand how the rocket works without studying what it left behind, how it got there, and how the energy may have been converted through the various stages to its final form.

### Flare emission and evolution

[Physical processes.](#) *Mon Feb 25 03:59:14 MST 2019*

Need to know general evolution of a flare, particularly the role of the chromosphere as we currently understand it. This is necessary in order to interpret the results from before, during, and after a flare; provides some context for what is physically happening.

An understanding of the physical processes that take place during solar flares ([when they happen, where they happen, the various structures involved, static physical conditions such as temperature, density, and composition, how much and why those values then change, etc.](#)) *18 October 2018* is crucial if one desires to characterize the role played by the relatively cool, thin atmospheric layer known as the chromosphere. These stages, as described by the standard model, provide vital context for the questions proposed, and then investigated for this dissertation, particularly the temporal behavior of the chromospheric 3-minute oscillations before, during, and after flares.

The development and evolution of the various dynamical phenomena that ultimately result in a solar flare takes place throughout the solar atmosphere in three primary

stages: precursor, impulsive, and gradual. Each of these are characterized by specific observations that are interpreted in the context of energy storage, release, and dissipation. The official time at which the event transitions from one stage to the next is determined by the SXR emission from the *GOES* satellite. GOES has two photometers that observe wavelength ranges 1-8Å (1.5-10 keV) and 0.5-4Å.

[Energy range for 0.5-4Å? Need source!](#) *18 October 2018*

These points in time are characterized by the initial increase, peak, and final return to background levels of the observed SXR flux. The times at which these features are observed in the lightcurves of other wavelength regimes in the EM spectrum tend to deviate from the *GOES* times since different processes in the course of flare development produce different types of emission during different stages.

Both the SXR and H $\alpha$  curves are observed to peak twice. a sharp increase at the onset (the impulsive phase), followed by a slower, smoother climb and subsequent decay (the gradual phase). Each phase is characterized by specific observations that are interpreted in the context of energy storage, release, conversion, and dissipation. These stages are important in understanding the role of the chromosphere, and provide the basis for the proposed investigation into the temporal localization of the chromospheric 3-minute oscillations.

Our current understanding of flares involves their development and evolution throughout the entire solar atmosphere. This is broken down into three main phases: the precursor, impulsive, and decay phases. Each of these are characterized by specific observations that are interpreted in the context of energy storage, release, and dissipation. These stages are important in understanding the role of the chromosphere, and will provide the basis for the proposed investigation into the temporal of the excitation of the chromospheric 3-minute oscillations.

**Pre-flare: the zero-th stage** According to the standard flare model ([source!](#) *date?*), the phenomenon we observe as a flare is the result of the rapid release of magnetic energy after days of slowing building to critical levels in the corona.

[Woods et al. \(2017\)](#) investigated the pre-flare stages of the March 29 flare in 2014 with IRIS and *Hinode*/EIS. [... And?](#) *18 October 2018*

[The following cute story was copied from Evernote, though probably came from proposal originally:](#) *18 October 2018*

Our journey begins during the “pre-flare” stage, during which magnetic energy builds to critical levels. This takes place over timescales from several days up to a few weeks. [Woods et al. \(2017\)](#) conducted a study to constrain the trigger mechanism of flares, for which there are several possibilities. They found plasma flows with velocities on

the order of several hundred km s<sup>-1</sup>. This is a key time period for space weather prediction.

*Testing :r! date to insert current date. Works! Although I'd prefer a different format... Thu Oct 18 14:58:21 EDT 2018*

**Precursor: the first stage** There are several possible mechanisms that could be responsible for triggering the release of the stored magnetic energy (see Woods et al. (2017) for an example).

The precursor phase, sometimes known as the pre-eruptive stage, begins when the release of magnetic energy is triggered. This stage typically lasts ~3 minutes. The eruption starts slowly, as the energy leaks slowly and the highly sheared magnetic field loses stability and begins to rearrange itself. The magnetic structure surrounding prominence evolves through series of force-free equilibria until it loses equilibrium and goes unstable. The plasma around the magnetic reconnection site heats up, and is observed as a slow increase in soft X-ray (SXR) and UV emission from active regions.

A sudden increases in speed occurs, most likely because the onset of magnetic reconnection releases field lines that were holding the prominence down, and cut it loose, hence the “activation of the prominence” (T-H and Emslie book).

This onset is important (e.g. SXR and UV before “cataclysmic onset of impulsive phase”). The magnetic field becomes unstable, starts to readjust. The emergence of new flux is now a thing. Prominence activation (Martin and Ramsey 1972) and heating of plasma (Poland et al. 1982; Hernandez et al. 1986; Klein et al. 1987; Machado et al. 1988a... from T-H & Emslie chapter 6?).

### **Impulsive: the second stage**

Once the magnetic configuration loses stability, an eruption occurs and stage two, the impulsive stage, begins. This stage only lasts for a minute or less. Magnetic reconnection begins, whose rapid onset is thought to be the cause of the sudden drop in evolutionary timescales from the precursor to the impulsive stage. There is a sudden release of energy that is then converted into various forms, including kinetic energy of accelerating particles, thermal energy that heats the plasma, bulk acceleration of fluid, and enhanced radiation fields. Intense radio, HXR, and gamma rays are emitted in the form of intense, rapidly fluctuating bursts. The jump in emission after it increased slowly during the precursor phase is thought to be caused by the rapid onset of MR. This process releases the prominence previously held down by the magnetic field. The prominence is the matter that is ejected outward in the form of a CME. [Priest & Longcope \(2017\)](#) distinguish two phases of magnetic reconnection. The first takes place during the impulsive phase, along the loop arcade, and is called “zipper reconnection”.

Once the magnetic configuration loses stability, an eruption occurs and stage two, the **impulsive** stage, begins. The onset of magnetic reconnection releases field lines previously holding the prominence down (Priest & Longcope 2017), and energy starts to be released at a much faster rate. Some of this energy is converted to kinetic energy of non-thermal particles, which are then accelerated down until they hit the chromosphere and inject the plasma with an impulsive burst of high energy ( $E \gtrsim 10$  keV). Energy is then lost to radiation in the form of intense, rapidly fluctuating bursts of radio, hard X-ray (HXR), and gamma rays. The HXR Bremsstrahlung radiation at the loop footpoints is indicative of energization of non-thermal particles, and this is where the initial heating of the chromospheric plasma takes place (Hooyng et al. 1981; Fletcher et al. 2013).

This entire process takes less than a minute. Many of the processes that take place during the impulsive phase are inferred from the response of the surrounding plasma, but cannot be observed directly due to the extremely short timescales over which they occur.

Magnetic energy released via magnetic reconnection is converted to kinetic energy of charged particles that are accelerated downward with energies exceeding 1 MeV.

After being injected into the denser plasma of the chromosphere, the interaction between NT electrons and the ambient particles causes the emission of Bremsstrahlung HXR radiation. This emission appears as ribbon-like features along the footpoints of the reconnected loops as they contract down into the lower atmosphere.

Chromospheric evaporation also occurs during this time. After the plasma is heated, some of the excess energy is shed by radiation or thermal conduction, but if these mechanisms are not enough to return the plasma to thermal equilibrium, the high gas pressure causes the plasma to rise up into the post-flare loops. Explosive evaporation occurs when the upward force is accompanied by an equal and opposite force in the opposite direction. This is revealed by the presence of redshifts in emission lines in addition to blueshifts. The downward movement of plasma is then referred to as chromospheric “condensation”. Velocities of plasma movement via explosive evaporation can be  $\gtrsim 100$  km s $^{-1}$ , and  $F_\ell > 10^{10}$  erg s $^{-1}$  cm $^{-2}$ .

Gentle evaporation refers to when the continuous, lower energy input from thermal conduction pushes plasma up the loops (evaporation), but not down (no condensation), so only blueshifts are observed. This process continues as long as a temperature gradient exists. Velocities of plasma movement via gentle evaporation are  $\gtrsim 10$  km s $^{-1}$ , and  $F_\ell < 10^{10}$  erg s $^{-1}$  cm $^{-2}$ .

## NT particle acceleration

Explosive can turn into gentle if conductive flux out of explosively heated plasma becomes comparable to energy flux in the electron beam:

$$F_{cond} \approx F_{NTe^-s}; \quad T \gtrsim 1 - \gtrsim 10s$$

**Gradual: the third and final stage** Once all the magnetic energy has been released and dissipated, non-thermal particles are no longer being accelerated downward, to drive chromospheric evaporation, and the gradual stage has begun. There remains a strong temperature gradient between the hot flare loops and the surrounding, cooler chromospheric plasma. Some of the energy that was not lost to radiation continues to heat the plasma via thermal conduction, which continues to drive evaporation of plasma upward through post-flare loops ([Battaglia et al. 2015](#)), though more slowly than during the impulsive phase. This final phase is characterized by a gradual buildup and decay of SXR emission from evaporation of hot post-flare loops. The loops continue to evolve by cooling and draining, and eventually retreat back down and become visible in H $\alpha$  ([Hudson 2007](#)). This emission reveals the morphology of the so-called “flare ribbons”. These are the footpoints of newly connected field lines, and are one of the primary observable features of flares. This stage typically lasts  $\sim$ 30 minutes.

### Flare classes

Flare are classified according to their peak soft x-ray flux (1-8Å), as measured at Earth from the *GOES* satellite. The classes are as follows:

- A:**  $10^4 < F < 10^3$
- B:**  $10^3 < F < 10^2$
- C:**  $10^2 < F < 10^1$
- M:**  $10^1 < F < 1$
- X:**  $1 < F < 10$

where  $F$  = flux ( $\text{erg s}^{-1} \text{cm}^2$ ). These are further subdivided from 1 through 9. This is a linear relationship so, for example, an X2 flare is twice as powerful as an X1 flare.

Typical flare temperatures are  $10^7$  K. Emission lines at these temperatures are blueshifted, while those at chromospheric or TR temperatures are redshifted ([Brosius et al. 2016](#)). Typical energies are around  $10^{27}10^{32}$  erg. The energy for the largest flares (i.e. of class  $>$  X10) has been capped at a few  $\times 10^{32}$  erg.

# THE SOLAR DYNAMICS OBSERVATORY (SDO)

## The Atmospheric Imaging Assembly (AIA)

The Atmospheric Imaging Assembly (AIA; Lemen et al. (2012)) on board the *Solar Dynamics Observatory* (SDO; Pesnell et al. (2012)) obtains full disk images throughout the solar atmosphere, using narrow band filters centered on 10 different wavelengths. Two of these channels provide measurements of thermal UV emission from the chromosphere. The 1700Å channel mostly contains continuum emission from the temperature minimum, and the 1600Å channel covers both continuum emission and the C IV spectral line in the upper photosphere and transition region. Both UV channels have a cadence of 24 seconds and spatial size scale of 0.6 arcseconds per pixel.

These data allow the computation of spatially resolved power maps centered on the frequency of interest.

### *Ambiguity in formation height*

**From proposals: date?** The Atmospheric Imaging Assembly (AIA) (Lemen et al. 2012; Boerner et al. 2012) on board *SDO* primarily collects EUV emission that originates in the corona. In addition it obtains thermal UV continuum data in two bandpasses centered on 1600Å and 1700Å. AIA 1700Å samples the lower atmosphere around  $T = 10^{3.7}$  K, close to  $T_{min}$ . AIA 1600Å samples the transition region and upper chromosphere, and contains emission from the C IV 1548Å line, as well as UV continuum. Both data sets are obtained at a cadence of 24 seconds, with a spatial resolution of  $\sim 0.6$  arcseconds per pixel.

**09 October 2018 - From current state of article (Phase 1): date?** The data used to analyze this flare is provided by AIA (Lemen et al. 2012), one of the instruments on board SDO (Pesnell et al. 2012). AIA obtains full disk images throughout the solar atmosphere using narrow band filters centered on 10 different wavelengths, two of which provide measurements of thermal UV emission from the chromosphere. The 1700Å channel mostly contains continuum emission from the temperature minimum, and the 1600Å channel covers both continuum emission and the C IV spectral line in the upper photosphere and transition region. Both channels have a cadence of 24 seconds and spatial size scale of 0.6 arcseconds per pixel.

## The Helioseismic and Magnetic Imager (HMI)

The Helioseismic and Magnetic Imager (HMI) is one of three instruments on board the *Solar Dynamics Observatory* (*SDO*). It obtains four types of filtergrams around

the Fe I line at 6173Å. These filtergrams are in the form of dopplergrams, vector magnetograms, line-of-sight magnetograms, and continuum intensity images (?).

Data from the Helioseismic and Magnetic Imager (HMI; [Scherrer et al. \(2012\)](#)), also on board *SDO*, is used to study potential correlations between magnetic field strength and oscillatory behavior in the chromosphere. HMI obtains full disk data in the form of line-of-sight magnetograms, vector magnetograms, Doppler velocity, and continuum intensity, measured at the Fe I absorption line at 6173Å with a passband width of 0.076Å. Each data product has a cadence of 45 seconds (with the exception of the vector magnetograms, at 135 seconds), and spatial size scale of 0.5 arcseconds per pixel ([Schou et al. 2012](#)).

## DATA REDUCTION AND ANALYSIS

Text.

### Alignment

Due to the global rotation of the sun, as well as smaller shifts caused by instrumental effects, it was necessary to apply an alignment procedure to the data cube.

The subset of data was extracted and aligned by cross correlation ([McAteer et al. 2003, 2004](#)). The associated routines provided sub-pixel accuracies.

### Saturation

### Analysis methods

# ENHANCED CHROMOSPHERIC 3-MINUTE OSCILLATORY POWER ASSOCIATED WITH THE 2011-FEBRUARY-15 X2.2 FLARE

## Introduction

### Observations and data reduction

Flare on 2011 February 15 took place “close to disk center”. How close is “close”? What are the difficulties in analyzing target close to the solar limb? Opacity issues? date?

The 2011 February 15 X2.2 flare occurred in NOAA active region (AR) 11158 close to disk center during solar cycle 24 (SOL2011-02-15T01:56). The AR was composed of a quadrupole: two sunspot pairs (four sunspots total). The X-flare occurred in a delta-spot composed of the leading spot of the southern pair and the trailing spot of the northern pair. It started at 01:44UT, peaked at 01:56UT, and ended at 02:06UT, as determined by the soft X-ray flux from the *Geostationary Operational Environmental Satellite* (*GOES*-15; [Viereck et al. \(2007\)](#)). The impulsive phase lasted about 10 minutes. Data covering 5 hours centered on this flare were used for the analysis. This data includes a C-class flare that occurred between 00:30 and 00:45 UT on 15 February 2011.

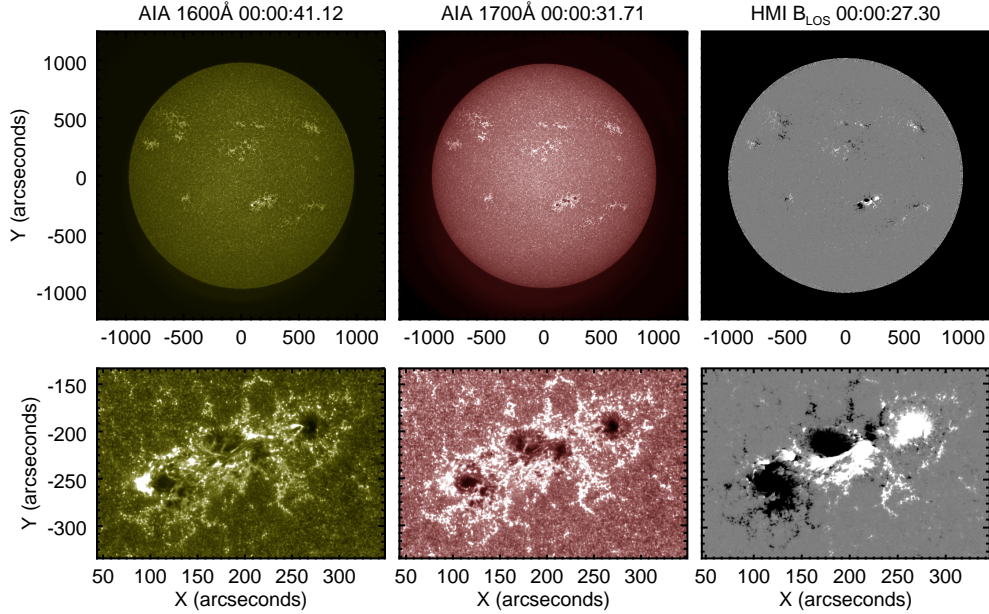


**Figure 1.** Images of active region 11158 in AIA 1600Å (left panels), AIA 1700Å (middle panels), and HMI LOS magnetogram (right panels), scaled to  $\pm 300$  Gauss. The top panels show the full disk (a nice example of the capabilities of AIA), and the bottom panels show the region used for analysis in this study.

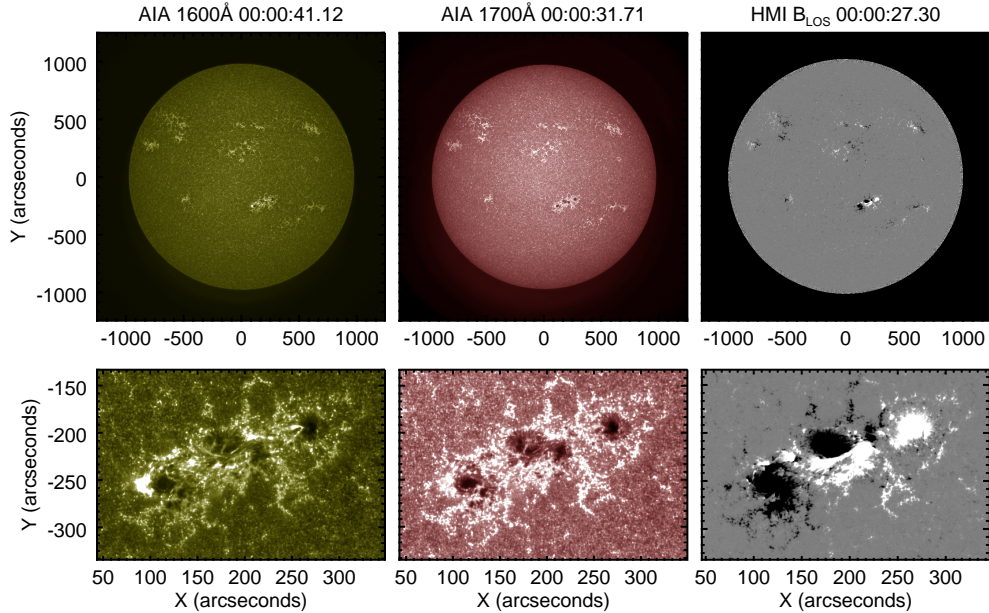


**Figure 2.** Images of active region 11158 in AIA 1600Å (left panels), AIA 1700Å (middle panels), and HMI LOS magnetogram (right panels), scaled to  $\pm 300$  Gauss. The top panels show the full disk, and the bottom panels show the region used for analysis in this study.

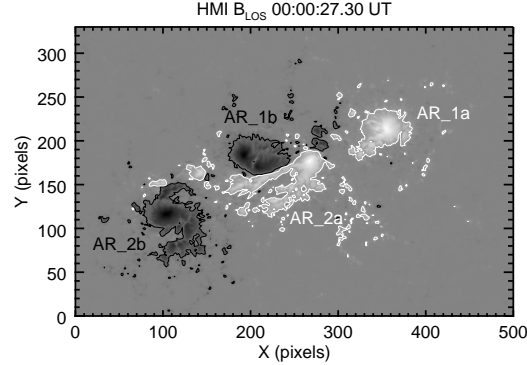


**Figure 3.** HMI LOS magnetogram. White and black contours outline positive (+300 Gauss) and negative (-300 Gauss) polarities, respectively. The two sunspots in the northern pair are labeled AR\_1a (leading sunspot) and AR\_1b (trailing sunspot). The two sunspots in the southern pair are labeled AR\_2a (leading sunspot) and AR\_2b (trailing sunspot).

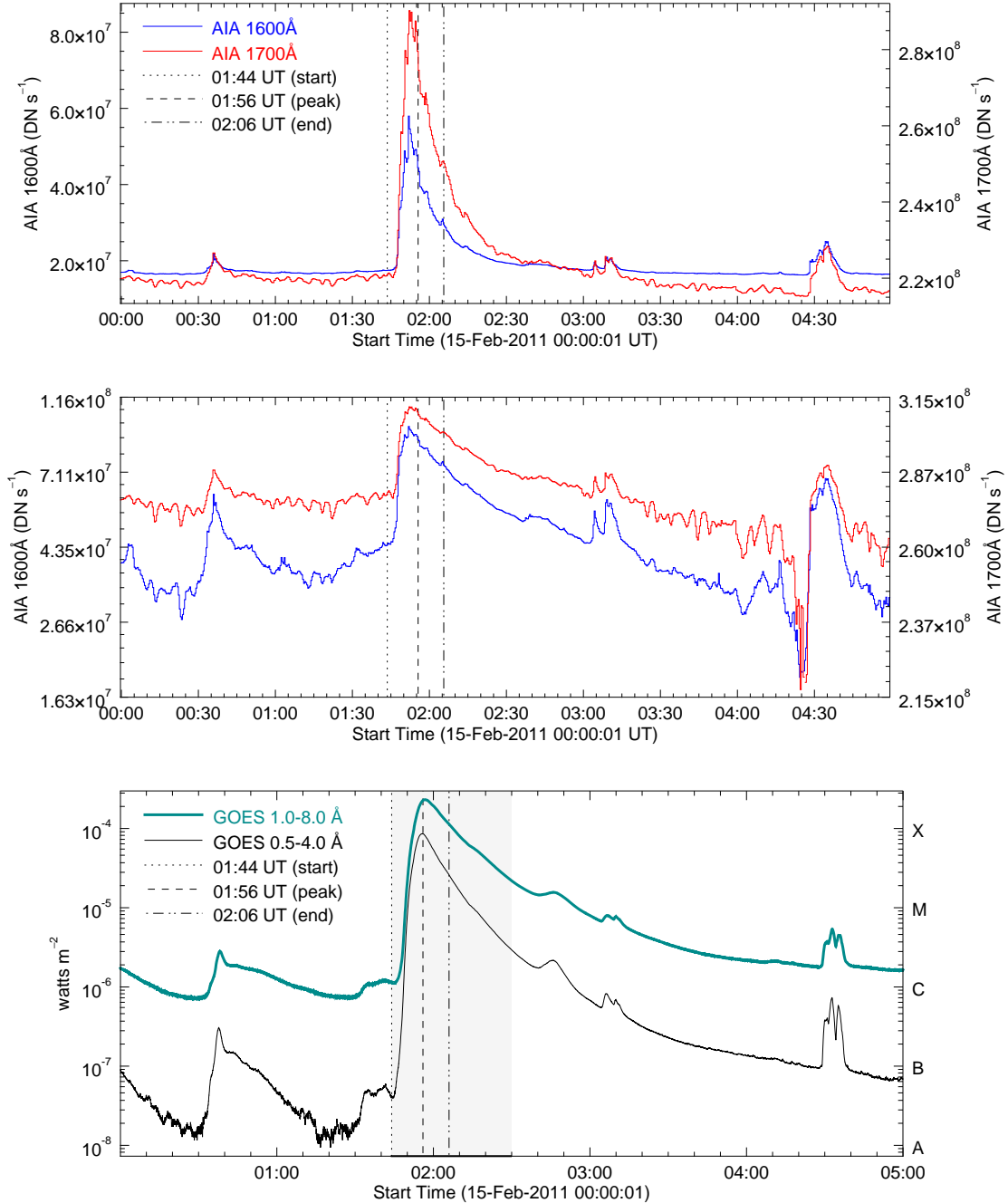


**Figure 4.** Top: Light curves of the UV continuum emission from AIA 1600Å (blue curve) and AIA 1700Å (red curve), integrated over the flare region in AR 11158. Middle: Same as top, but scaled as log(flux). Bottom: Light curves from *GOES-15* channels 1-8Å (black curve) and 0.5-4Å (pink curve), scaled as log(flux) to enable visibility of the increases during smaller events before and after the main X-flare.

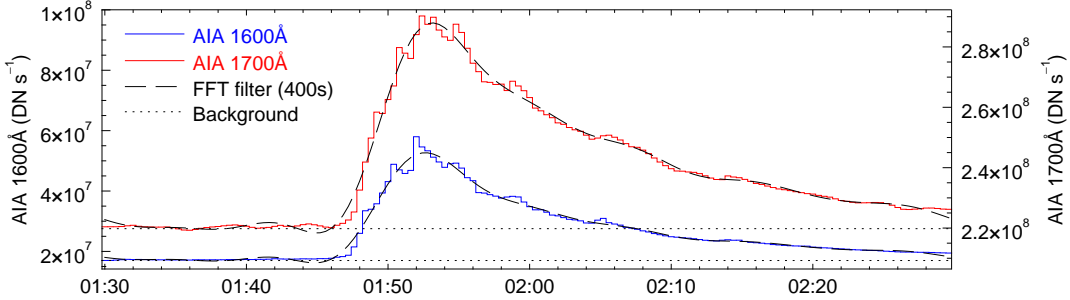


**Figure 5.** Light curves of AIA 1600Å and AIA 1700Å, overlaid with same light curves after applying an FFT filter with a period cutoff of 400 seconds.

Plot of detrended data goes here. Threshold = lower limit on frequency to get rid of global variations (e.g. the flare) and keep high-frequency variations, like QPPs. Sun Dec 2 12:37:06 MST 2018

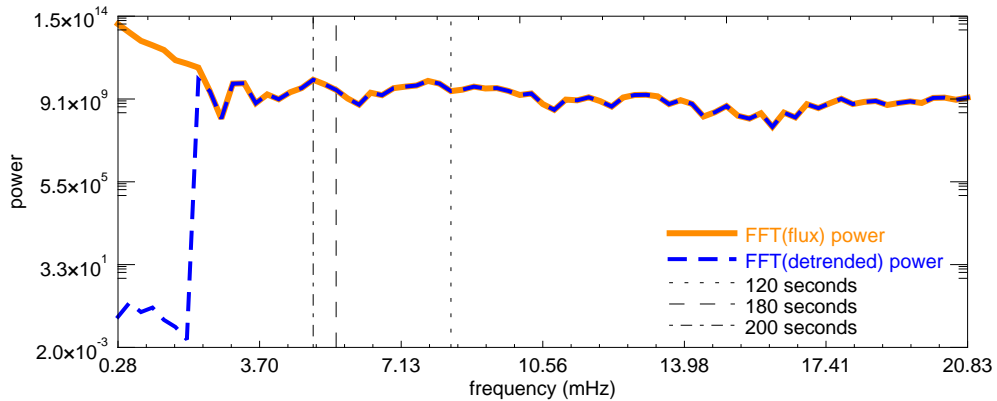


**Figure 6.** Power spectrum from AIA 1600Å flux between 1:30 and 2:30 UT. The orange curve is the power from the raw data, and the blue curve is the power from flux after applying an FFT high-pass filter to remove variations with periods longer than 400 seconds, such as the global flare curve, which dominates the spectrum at low frequencies.

Figure 4 shows light curves for the full 5-hour time series from 00:00 to 04:59 on 2011-February-15. The top panel shows both AIA channels. The bottom panel shows both SXR channels from *GOES-15* at 1-8Å (black curve) and 0.5-4Å (pink curve). A small C-flare occurred before the X-flare between 00:30 and 00:45 UT, and two small events occurred after the X-flare, between 03:00 and 03:15, and between 04:25 and 04:45.

Pre-flare images of the full disk are shown in Figure 1, along with a 300x198 arcsecond subset of the data centered on AR 11158. This subset was extracted and aligned by cross correlation (McAteer et al. 2003, 2004). Images were scaled to improve contrast using the *aia\_intscale.pro* routine from *sswidl*. The magnetic configuration of the quadrupole is clear in the HMI magnetograms. The northern pair will be designated as AR\_1 and the southern pair will be designated as AR\_2. Sunspots in the northern

pair will be designated as AR\_1a (positive polarity) and AR\_1b (negative polarity). Sunspots in the southern pair will be designated as AR\_2a (positive polarity) and AR\_2b (negative polarity).

Both AIA channels saturated ( $\geq 15000$  counts) in the center during the peak of the X-class flare, and a few pixels also saturated during the smaller events before and after. Affected pixels were all contained within the 300x198 arcsecond subset of data throughout the duration of the time series. Four images from the 1700Å channel on AIA were missing, between the images with start times at 00:59:53.12, 01:59:29.12, 02:59:05.12, and 03:58:41.12, and the following images, each with start times 48 seconds after the previous image. Since the gaps in data were separated by an hour, it was reasonable to approximate missing images by averaging the two adjacent images.

## Analysis

## Results and discussion

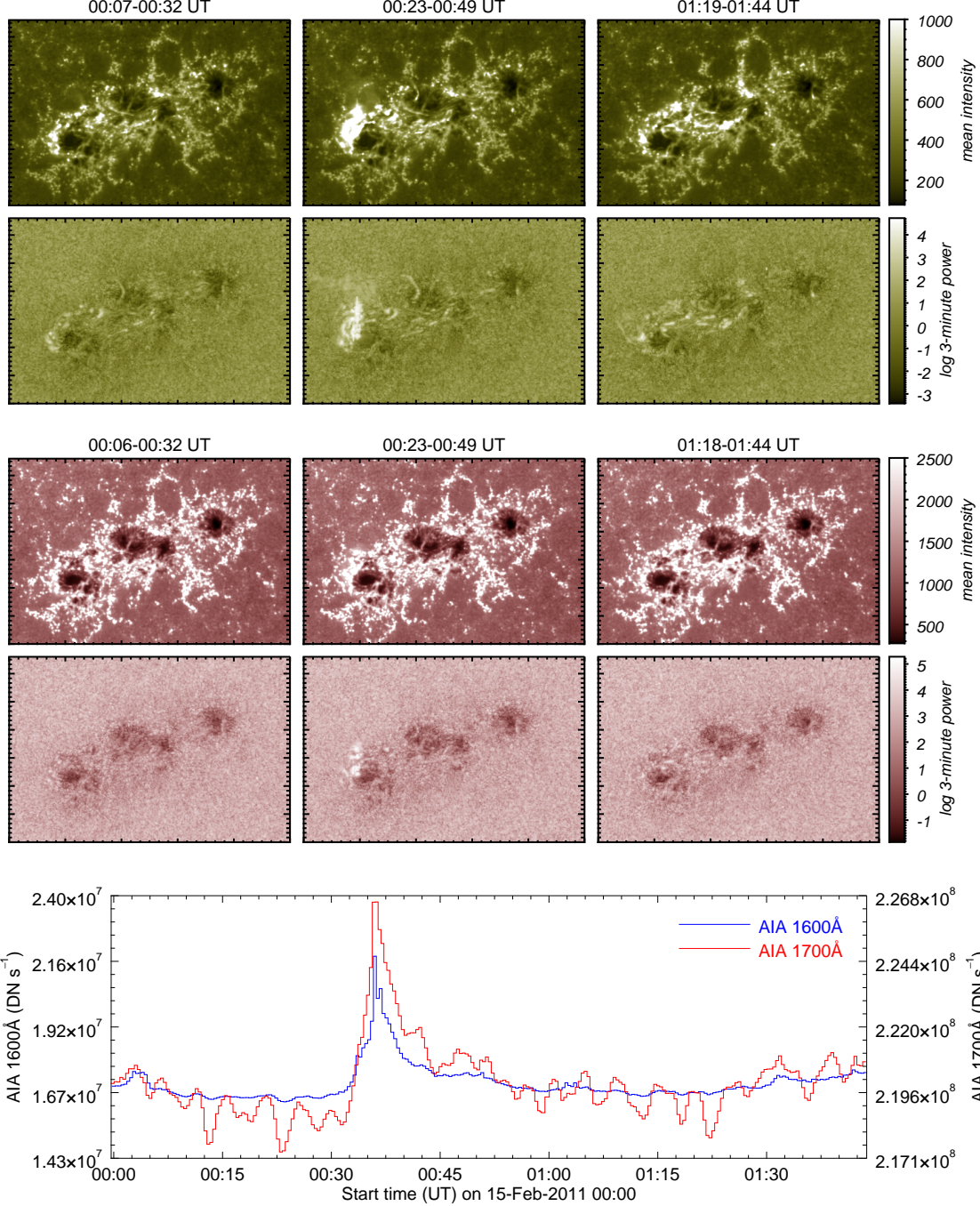


**Figure 7.** Spatial distribution of 3-minute power (arbitrary instrumental units) for AIA 1600Å (top) and AIA 1700Å (bottom) with the central frequency at 5.6 mHz ( $\pm 0.5$  mHz). The  $x$  and  $y$  dimensions are the same as the images in Figure 1.

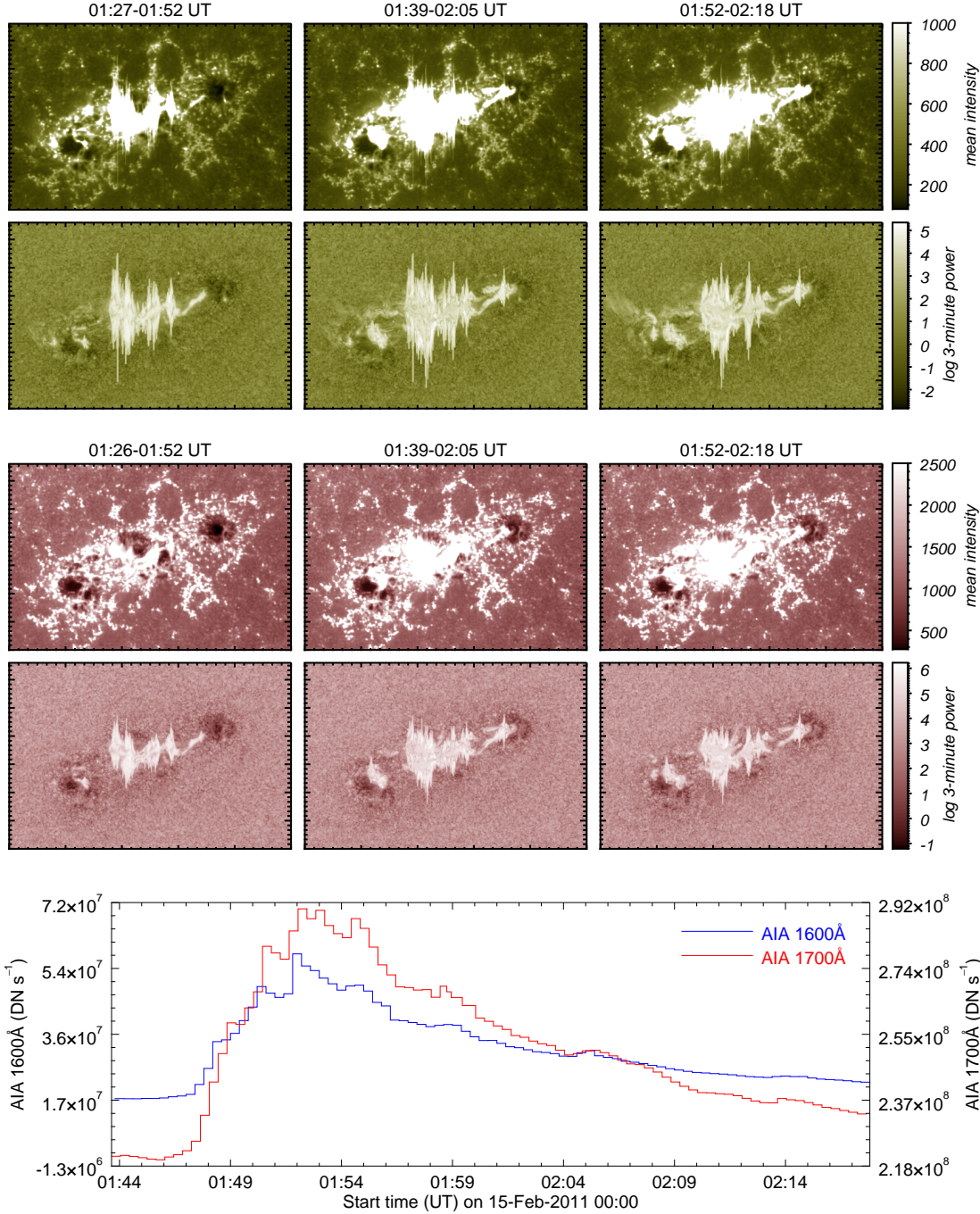
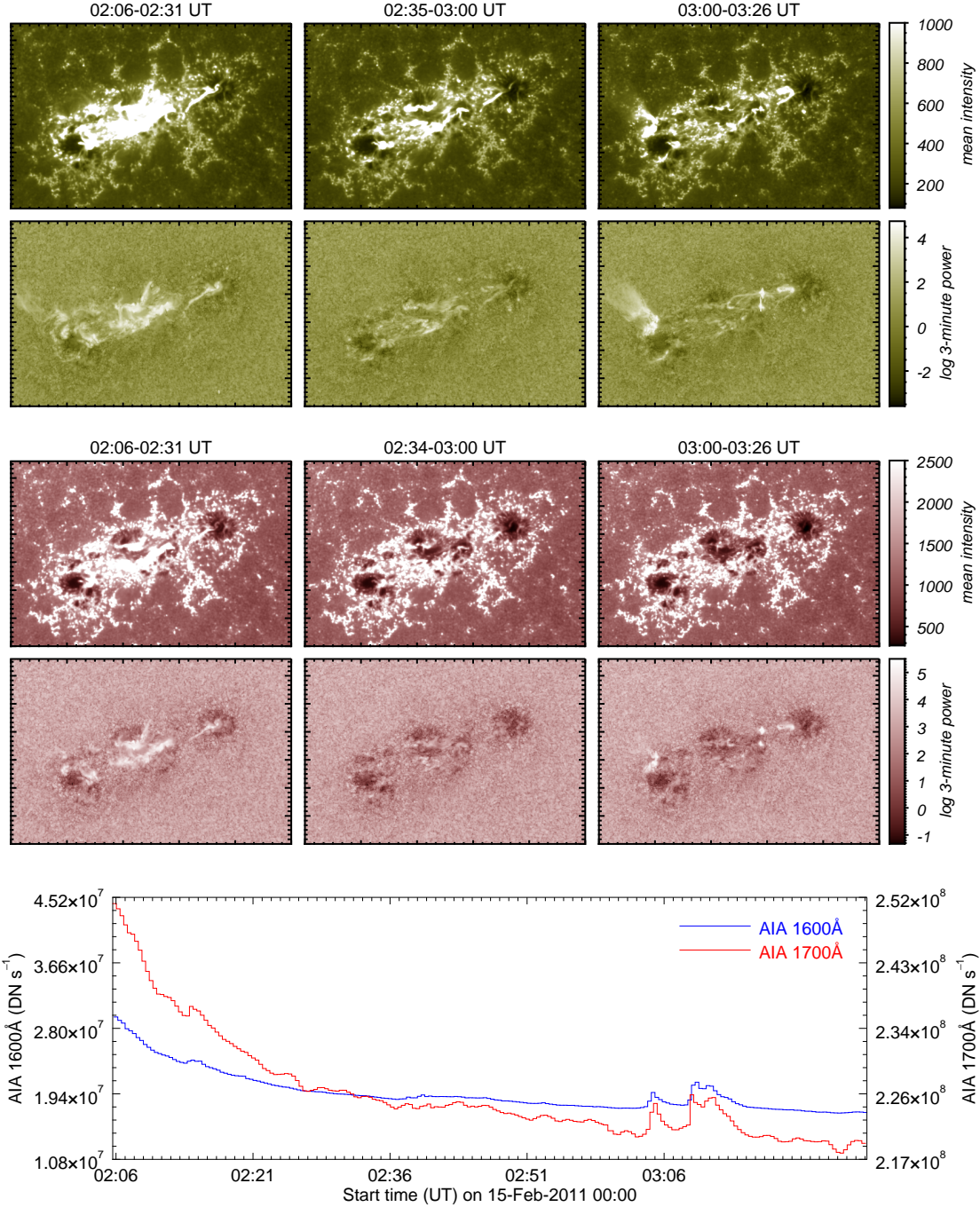
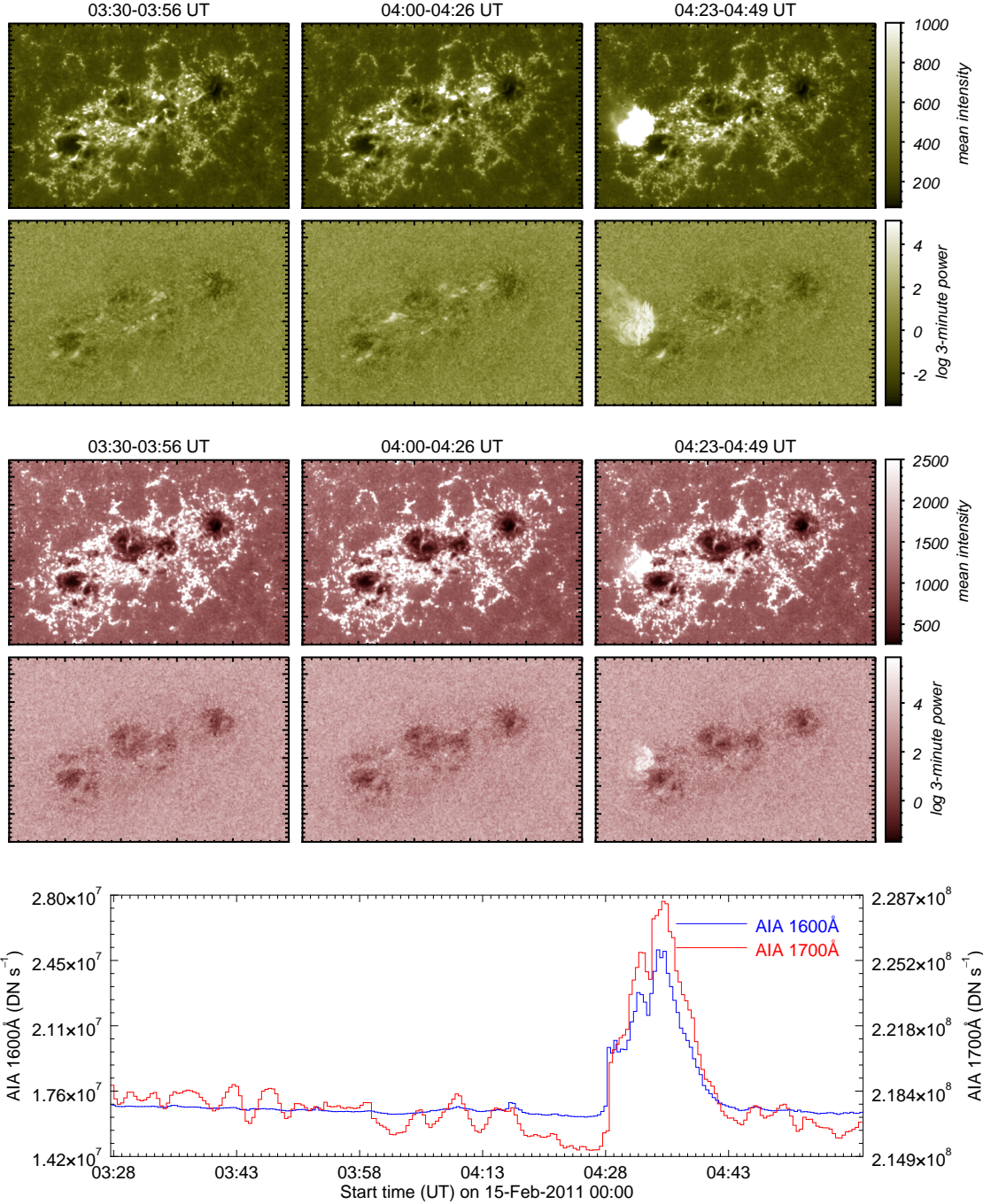


Figure 8. Mid-flare power maps.



**Figure 9.** Post-flare power maps.



**Figure 10.** Post-flare power maps.

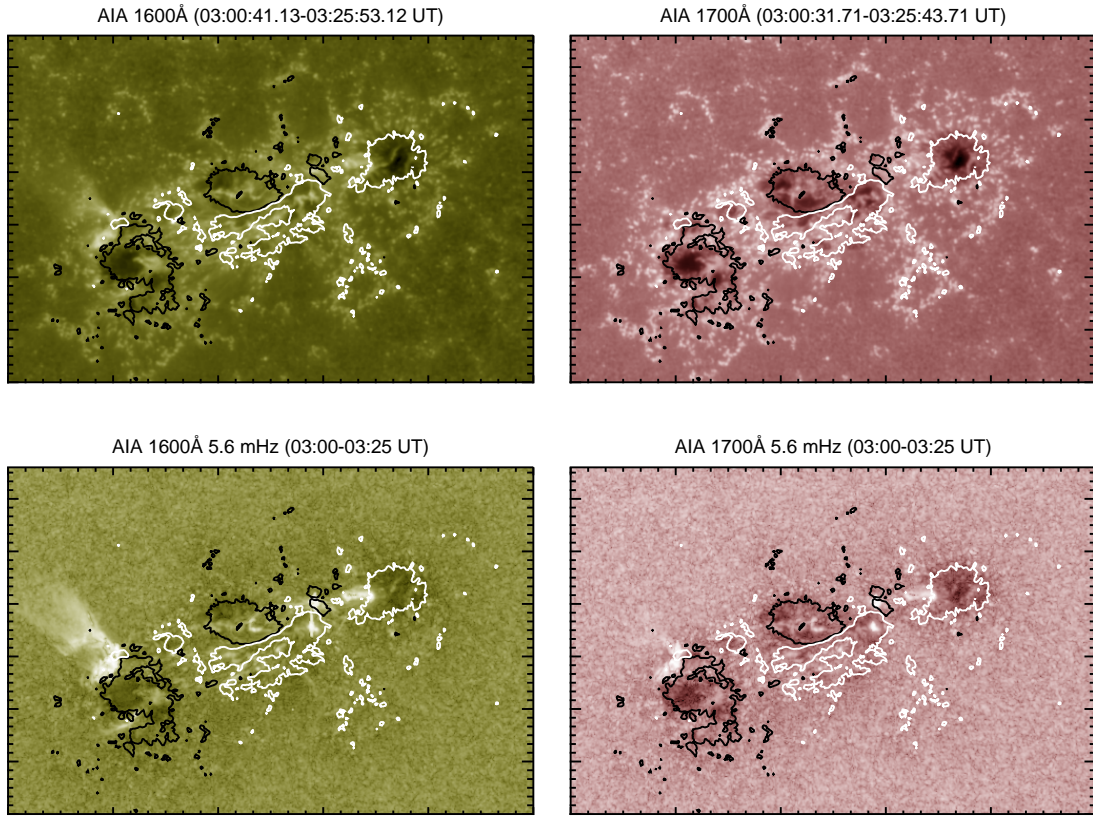


**Figure 11.** Post-flare power maps overlaid with contours showing the approximate location of the  $B_{LOS}$  at  $\pm 300$  Gauss. White and black contours represent positive and negative polarity, respectively.

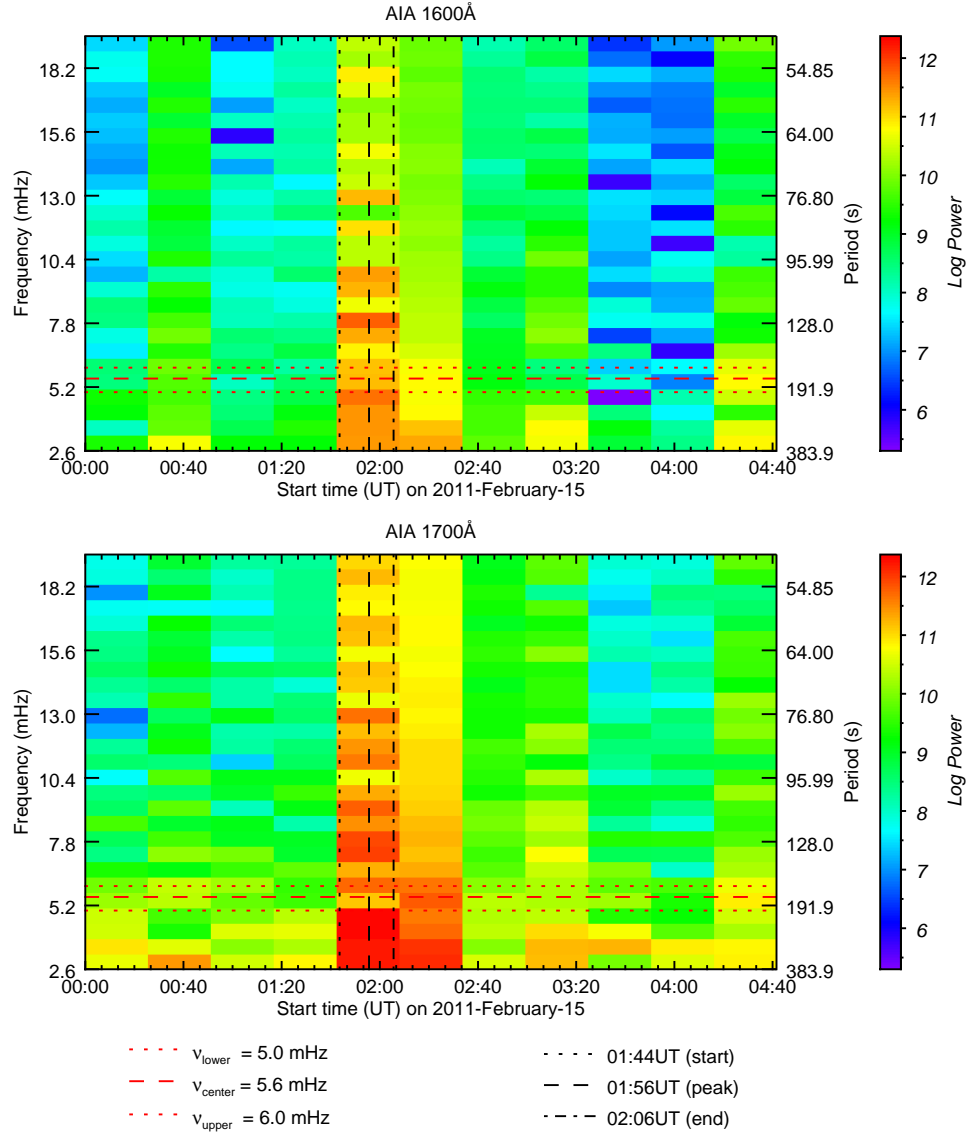


**Figure 12.** Time-frequency power plots from AIA 1600 $\text{\AA}$  (top panel) and AIA 1700 $\text{\AA}$  (bottom panel), obtained by applying a Fourier transform to integrated emission from NOAA AR 11158 in discrete time increments of 64 frames ( $\sim 25.6$  minutes) each. The dashed horizontal line marks the central frequency  $\nu_c$  at  $\sim 5.6$  mHz, corresponding to a period of 3 minutes. The dotted horizontal lines on either side of  $\nu_c$  mark the edges of the frequency bandpass  $\Delta\nu = 1$  mHz. The vertical lines mark the flare, start, peak, and end times as determined by *GOES*. The power is scaled logarithmically and over the same range in both channels. Note that the x-axis labels do not necessarily line up with the boundaries of the data columns.

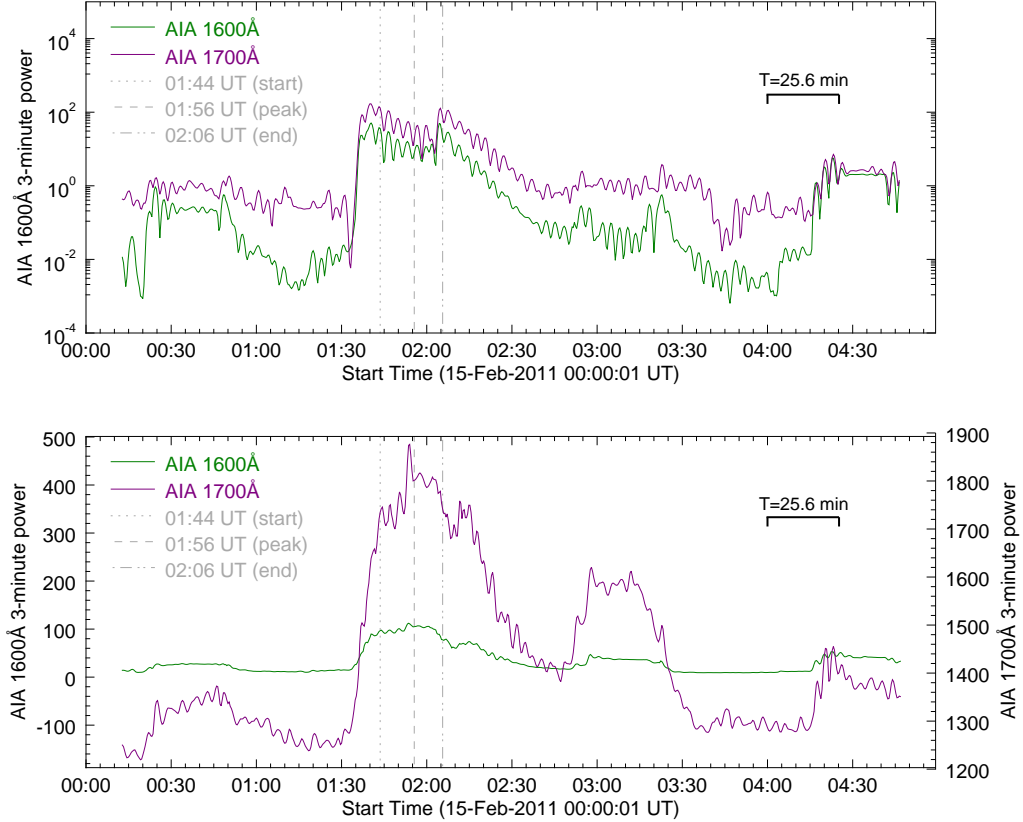
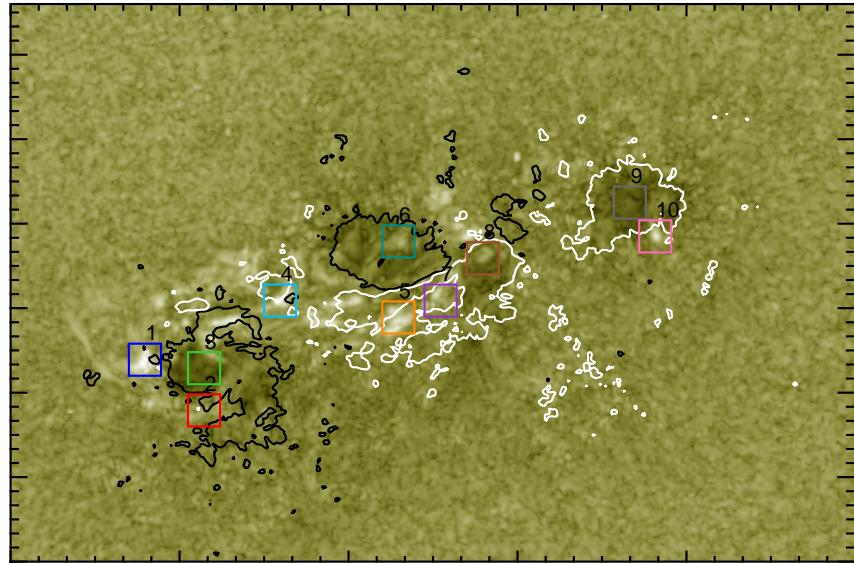
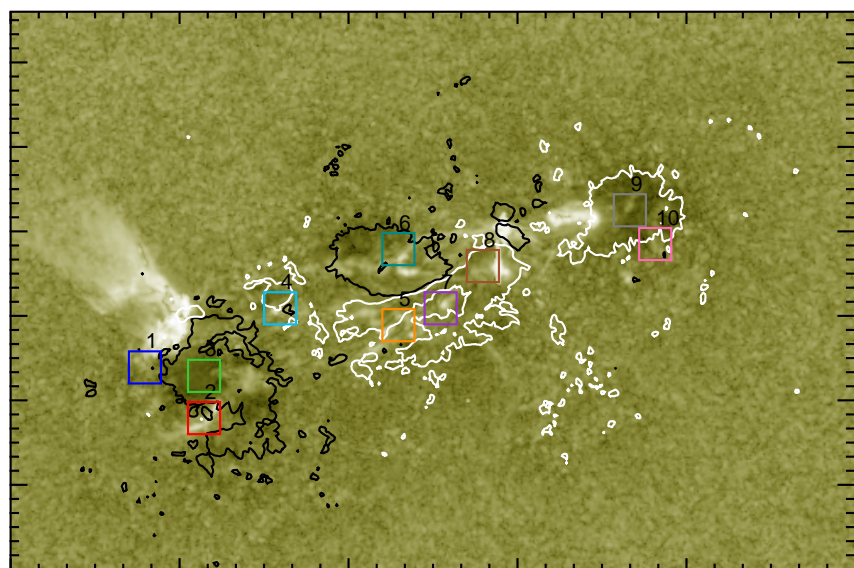


**Figure 13.** Temporal evolution of the 3-minute power  $P_{3\text{min}}(t)$  in AIA 1600 $\text{\AA}$  (blue curve) and AIA 1700 $\text{\AA}$  (red curve). Top:  $P(t)$  obtained by applying a Fourier transform to the integrated flux from AR 11158. Bottom:  $P(t)$  per unsaturated pixel, obtained by summing over power maps. Each point in time is plotted as a function of the center of the time segment over which the Fourier transform was applied to obtain the power map over which the point was summed. The vertical dashed lines mark the *GOES* start, peak, and end times of the flare at 01:44, 01:56, and 02:06 UT, respectively.

AIA 1600Å 5.6 mHz (01:19-01:44 UT)



AIA 1600Å 5.6 mHz (03:00-03:25 UT)



## Conclusions

## APPENDIX: PHYSICS BACKGROUND

### Waves

1D:

$$\frac{\partial^2 \psi}{\partial x^2} - \frac{1}{v^2} \frac{\partial^2 \psi}{\partial t^2} = 0$$

3D:

$$\frac{\partial^2 \psi}{\partial x^2} \rightarrow \nabla^2 \psi$$

propagation speed  $v$ :

$$v = \sqrt{\frac{F_r}{\rho}}$$

$F_r$  = restoring “force”;  $\rho$  = mass “density”

Get solutions to wave equation by specifying:

- ICs - prescribe amplitude and phase
- BCs - solutions are standing waves, or harmonics

$$\left( \nabla^2 - \frac{1}{c^2} \frac{\partial^2}{\partial t^2} \right) \psi(\vec{r}, t) = 0$$

## The acoustic cutoff frequency

In the interior of the sun, acoustic waves have frequencies higher than the cutoff, so it is of less importance there. In the solar atmosphere, however, the cutoff plays an important role in the behavior of waves and oscillatory phenomena. The cutoff peaks in the chromosphere, at a value of about 5.5 mHz, or roughly three minutes. This is also the dominant frequency of the oscillations observed everywhere at all times in the chromosphere.

If waves with frequencies lower than the cutoff are unable to propagate at a certain height, then one would expect to see a continuously high power spectrum at frequencies higher than this, and then a drop to zero at frequencies lower than this. However, what we see is a peak at the cutoff, but the power drops again for higher frequencies.

[Where are the higher frequencies? date?](#)

This may be because waves at higher frequencies simply aren't generated in the first place.

[If the cutoff frequency didn't exist, how would power at lower frequencies compare to the 3-minute power? Higher or lower? Or do these waves even exist to begin with? date?](#)

[What types of waves are generated in the atmosphere, and why? date?](#)

Figure

reffig:Stangalini2011 shows power maps from [Stangalini et al. \(2011\)](#) illustrating the power distribution of the 3-minute oscillations at the photospheric Fe 6173 Å line and the chromospheric Ca 8542 Å line. Also shown is the power distribution of the 5-minute oscillations. The 5-minute period has been attributed to the global pulsations of the sun due to pressure modes (*p*-modes) in the interior. The image shows the suppression of the 5-minute period in the umbra of sunspots, the opposite of the 3-minute behavior in the chromosphere above sunspots. It is commonly observed in the photosphere that the 5-minute power above sunspot umbrae is *reduced* compared to the quiet sun by a factor of 2-5, though it is still the dominant frequency ([Felipe et al. 2010; Bogdan & Judge 2006](#)). [Reznikova et al. \(2012\)](#) also observed lowering of the cutoff frequency due to inclination of magnetic field lines. The presence of the 5-minute oscillations in the diffuse magnetic regions surrounding the umbra is likely caused by the decrease in effective cutoff frequency due to the inclination of the magnetic field. Waves that are generated in the lower atmosphere propagate upward until their frequency no longer exceeds the local cutoff frequency and they are reflected ([De Moortel et al. 2000; Brynildsen et al. 1999](#)). The cutoff frequency at the base of the chromosphere is  $\sim$ 5.5 mHz, or roughly 3 minutes, which agrees with

the acoustic cutoff period of a gas with the composition and pressure scale height of the upper photosphere (Kalkofen 1994).

Waves with a frequency lower than the cutoff will:

- be reflected back down
- shock and dissipate
- strongly damp out

What is the 'natural frequency', and what is the significance of the chromosphere oscillating at its natural frequency (as opposed to . . .)? Milligan paper presented evidence supporting that the chromosphere oscillates at its natural frequency in response to a disturbance, but never stated why this is significant or the implications for bigger picture science. date?

### ***Derivation of the cutoff frequency***

The cutoff frequency defines the minimum frequency a wave must have in order to propagate through a medium. It is an intrinsic property of the medium, determined by local macro parameters, such as pressure and density. As these properties vary throughout the interior of the sun and its atmosphere, the cutoff frequency itself is an indirect function of height.

*Plot of cutoff frequency with height goes here. date?*

Acoustic waves obey the Klein Gordon equation:

$$\frac{\partial^2 u}{\partial t^2} - (c_s^2) \frac{\partial^2 u}{\partial z^2} + \Omega^2 u = 0 \quad (4)$$

where  $u$  = velocity amplitude,  $t$  = time,  $c_s$  = local sound speed,  $z$  = height above the photosphere, and where  $\Omega = 2\pi\nu_{ac}$  is the cutoff frequency in radians per second ( $\nu_{ac}$  = cutoff frequency in oscillations per second),

The solution for  $u$  is of the form:

$$u = u_0 e^{i(k_z z - \omega t)} \quad (5)$$

where  $\omega = 2\pi f$  is the oscillation frequency of the wave in radians s<sup>-1</sup> ( $f$  = frequency in Hz), and  $k_z = 2\pi/\lambda$  is the wavenumber in the  $z$ -direction. Using this solution, we eventually get:

$$c_s^2 k^2 = \omega^2 - \Omega^2 \quad (6)$$

If  $\omega < \Omega$ , then  $k^2 < 0$  and  $k$  is imaginary. In this case, the wave cannot propagate and standing oscillations are observed.

$$\Omega = \frac{c_s}{2H} \quad (7)$$

$H$  = scale height.

$$\Omega = \frac{c_s}{2H} = 2\pi\nu_{ac} \quad (8)$$

$$\nu_{ac} = \frac{c_s}{4\pi H} \quad (9)$$

$$\nu_{ac} = \sqrt{\frac{\gamma k T}{16\pi^2 H^2 \mu m_{amu}}} \quad (10)$$

where  $c_s$  is given by:

$$c_s = \sqrt{\frac{\gamma P}{\rho}} = \sqrt{\frac{\gamma kT}{\mu m_{amu}}} \quad (11)$$

Setting  $\gamma$  to 5/3,  $\mu = 1.2$ ,  $H = 150$  km, and  $T = 4200$  K (the approximate temperature minimum), the acoustic cutoff frequency  $\nu_{ac}$  comes out to roughly 5.6 mHz, the frequency at which the 3-minute chromospheric period oscillates.

I assume the following is very similar to the above text, but don't feel like looking at it closely right now... Mon Feb 18 17:15:24 MST 2019

The cutoff frequency of a medium is determined by local macro parameters, such as pressure and density. Waves that oscillate with a frequency higher than this will propagate through the medium, whereas waves with a frequency lower than the cutoff will shock and dissipate. Acoustic waves obey the Klein Gordon equation:

$$\frac{\partial^2 u}{\partial t^2} - (c_s^2) \frac{\partial^2 u}{\partial z^2} + \Omega^2 u = 0 \quad (12)$$

where  $\Omega = c_s/2H_P$  is the cutoff frequency ( $c_s$  is the local sound speed and  $H_P = kT/\mu g$  is the pressure scale height),  $t$  is time,  $z$  is height above the photosphere, and  $u$  is the velocity amplitude. The solution for  $u$  is of the form:

$$u = u_0 e^{i(k_z z - \omega t)} \quad (13)$$

where  $\omega = 2\pi\nu_{ac}$  is the oscillation frequency of the wave in radians s<sup>-1</sup> ( $\nu_{ac}$  = acoustic wave frequency in Hz), and  $k_z = 2\pi/\lambda$  is the wavenumber in the  $z$ -direction. Using this solution yields:

$$c_s^2 k^2 = \omega^2 - \Omega^2 \quad (14)$$

If  $\omega < \Omega$ , then  $k^2 < 0$  and  $k$  is imaginary. In this case, the wave cannot propagate and standing oscillations are observed.

$$2\pi\nu_{ac} = \frac{c_s}{2H_P} = \Omega \quad (15)$$

$$\nu_{ac} = \frac{c_s}{4\pi H_P} = \sqrt{\frac{\gamma kT}{16\pi^2 H_P^2 \mu m_{amu}}} \quad (16)$$

where  $c_s$  is given by:

$$c_s = \sqrt{\frac{\gamma P}{\rho}} = \sqrt{\frac{\gamma kT}{\mu m_{amu}}} \quad (17)$$

Setting  $\gamma = 5/3$ ,  $\mu = 1.2$  amu,  $H_P = 150$  km, and  $T = T_{min} \approx 4200$  K, the acoustic cutoff frequency  $\nu_{ac}$  comes out to roughly 5.5 mHz, which corresponds to  $\sim 3$  minutes.

The numerical value of the cutoff frequency depends on physical parameters of the ambient environment, such as composition, temperature, and pressure scale height.

## Coronal seismology

### *Ideal MHD*

Conditions of “ideal MHD” involve timescales between collision that are much smaller than those of other processes, allowing the particles to take a Maxwellian distribution. They describe the evolution of the plasma densities (mass, energy, etc.) over time. Under conditions of ideal MHD, plasma acts as a perfect conductor, and is completely frozen-in to the magnetic field lines.

The equations of ideal MHD are shown in Table ref{tab:idealMHD}.  
inputtable\_idealMHD

Figure ref{disp} shows the location of the different MHD modes relative to characteristic speeds both external to and inside a cylindrical volume of plasma.

### *Characteristic speeds*

Relations between the (internal and external) characteristic speeds (Alfvén, sound, and tube speeds) determine properties of MHD modes guided by the tube.

1. Sound speed:  $C_s = \sqrt{\frac{\gamma p_0}{\rho_0}} \approx 166 T_o^{1/2} \text{ m s}^{-1} = 200 \text{ km s}^{-1}$   
(All sound speeds  $\approx \sqrt{\frac{ED}{\rho_I}}$  ), where  $\rho_I$  = inertial mass density.  
ED of magnetosphere  $= \frac{B^2}{2\mu_0} = \frac{P}{\rho}$   
 $C_s = \sqrt{\frac{P\gamma}{\rho}}$

2. Alfvén speed = “speed at which hydrodynamic waves can be propagated in a magnetically dominated plasma.” [Source?](#) 07/17/17 15:21

$$C_A = \frac{B_0}{\sqrt{\mu_0 \rho_0}}$$

$$V_A = 2.18 \times 10^{12} \frac{B_o}{\sqrt{n_o}} \text{ m s}^{-1} = 3000 \text{ km s}^{-1}$$

$$(B_o \sim 100 \text{ G}; n_o \sim 10^{16} \text{ m}^{-3})$$

3. Tube/Cusp speed:  $C_T = C_s C_A / (C_A^2 + C_s^2)^{1/2}$  = combination of sound and Alfvén speeds

Audible hearing limit:  $C_s = 20 \text{ Hz}$ . In space,  $\nu \approx 10^{-7} \text{ Hz}$ .

### **Kink waves**

#### *Speed*

In the long wavelength limit, the phase speed of all but sausage fast modes (see below) tends to the so-called kink speed, which corresponds to the density weighted average Alfvén speed. Phase speed for kink waves is equal to this kink speed,  $c_k$ :

$$v_{ph} = c_k = \sqrt{\frac{\rho_o V_{Ao}^2 + \rho_e V_{Ae}^2}{\rho_o + \rho_e}} \approx V_A \sqrt{\frac{2}{1 + \frac{\rho_e}{\rho_o}}}$$

in the low- $\beta$  plasma.

Frequency:

$$w_K = \sqrt{\frac{2k_z B^2}{\mu(\rho_i + \rho_e)}}$$

Slab phase speed:

$$V_{Ae}$$

Tube kink speed:

$$c_K = \frac{B_i^2 + B_e^2}{\sqrt{\mu(\rho_i + \rho_e)}}$$

(mean Alfvénic speed). Slab (or tube) is moved laterally; little variation in cross-sec, density, or intensity.

#### *Period*

$$P = \frac{2\ell}{V_A} \sqrt{\frac{1 + \rho_e/\rho_o}{2}}$$

where  $\lambda = 2\ell$  ( $\ell$  is the loop length). Typically,  $\ell \approx 60 - 600$  Mm in the corona.

Period of global kink mode:

$$P = \frac{2\ell}{c_K}$$

where  $P \approx$  few seconds - minutes

### Thermal and non-thermal energy

Thermal energy is radiated by matter in *thermal equilibrium*. The extreme ends of the spectrum (radio and HXR) are dominated by radiation from non-thermal particles in the early stages of flare energy release, but the intermediate regimes (visible, EUV, and SXR) are dominated by radiation from thermal particles during the decay period, over longer timescales. Figure

reffig:nt shows a comparison between the two types of energy across the electromagnetic spectrum. Non-thermal particles are revealed by observed energies that, if caused by thermal particles, would indicate temperatures far higher than observed, according to

$$E_{\text{thermal}} = \frac{3}{2}k_B T \quad (18)$$

where  $k_B = 1.38 \times 10^{-16}$  = Boltzmann's constant in erg K<sup>-1</sup>,  $T$  = temperature in Kelvin, and  $E_{\text{thermal}}$  = thermal energy in erg. The distinction between thermal and non-thermal particles is important when diagnosing observations. They result from different processes and provide clues to the conditions in their environment.

## NORMALIZATION OF POWER SPECTRUM

Figure ?? shows power spectra for each AIA channel during the X-class flare and during the pre-flare period. These were calculated with and without normalizing to see which method was best for the type of analysis utilized in this work.

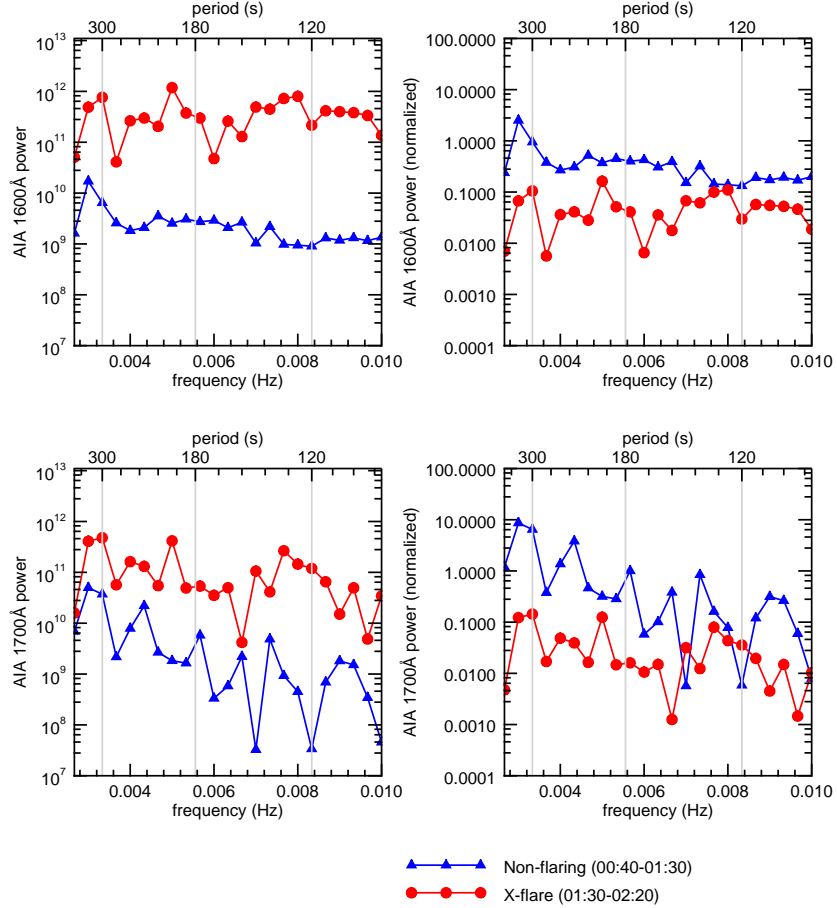


**Figure 14.** Fourier power spectrum for quiet vs. flaring times, comparing calculations without normalizing (left panels) to those with normalizing (right panels) for both AIA 1600Å (top) and AIA 1700Å (bottom). All spectra were obtained by applying a Fourier transform to the integrated emission from AR 11158.

## REFERENCES

- Battaglia, M., Kleint, L., Krucker, S., & Graham, D. 2015, *Astrophys. J.*, 813, 113, doi: [10.1088/0004-637X/813/2/113](https://doi.org/10.1088/0004-637X/813/2/113)
- Beckers, J. M., & Schultz, R. B. 1972, *Sol. Phys.*, 27, 61, doi: [10.1007/BF00151770](https://doi.org/10.1007/BF00151770)
- Beckers, J. M., & Tallant, P. E. 1969, *Sol. Phys.*, 7, 351, doi: [10.1007/BF00146140](https://doi.org/10.1007/BF00146140)
- Boerner, P., Edwards, C., Lemen, J., et al. 2012, *Sol. Dyn. Obs.*, 9781461436, 41, doi: [10.1007/978-1-4614-3673-7\\_4](https://doi.org/10.1007/978-1-4614-3673-7_4)
- Bogdan, T. J., & Judge, P. G. 2006, *Philos. Trans. R. Soc.*, 364, 313, doi: [10.1098/rsta.2005.1701](https://doi.org/10.1098/rsta.2005.1701)
- Brosius, J. W., Daw, A. N., & Inglis, A. R. 2016, *Astrophys. J.*, 830, 101, doi: [10.3847/0004-637X/830/2/101](https://doi.org/10.3847/0004-637X/830/2/101)
- Brynildsen, N., Leifsen, T., Kjeldseth-Moe, O., Maltby, P., & Wilhelm, K. 1999, *\Apjl*, 511, L121, doi: [10.1086/311854](https://doi.org/10.1086/311854)
- Brynildsen, N., Maltby, P., Fredvik, T., & Kjeldseth-Moe, O. 2004. <http://adsabs.harvard.edu/abs/2004ESASP.547...45B>
- Chae, J., & Goode, P. R. 2015, *Astrophys. J.*, 808, 118, doi: [10.1088/0004-637X/808/2/118](https://doi.org/10.1088/0004-637X/808/2/118)
- De Moortel, I., Ireland, J., & Walsh, R. 2000, *Astron. Astrophys.*, 355, L23, doi: [10.1063/1.1324943](https://doi.org/10.1063/1.1324943)
- Felipe, T., Khomenko, E., & Collados, M. 2010, *Astrophys. J.*, 719, 357, doi: [10.1088/0004-637X/719/1/357](https://doi.org/10.1088/0004-637X/719/1/357)
- Fleck, & Schmitz. 1991, *Astron. Astrophys.*, 250, 235
- Fletcher, L., Hannah, I. G., Hudson, H. S., & Innes, D. E. 2013, *Astrophys. J.*, 771, 104, doi: [10.1088/0004-637X/771/2/104](https://doi.org/10.1088/0004-637X/771/2/104)
- Giovanelli. 1972, *Sol. Phys.*, 27, 71
- Hoyng, P., Duijveman, A., Machado, M. E., et al. 1981, *Astrophys. J. Lett.*, 246, L155, doi: [10.1086/183574](https://doi.org/10.1086/183574)
- Hudson, H. 2007, *Phys. Chromospheric Plasmas*, 368, 365. <https://arxiv.org/abs/0704.0823>
- Jensen, & Orrall, F. Q. 1963
- Judge, P. 2006, *Sol. MHD Theory Obs. A High Spat. Resolut. Perspect.*, 354, 259. <https://arxiv.org/abs/0701379>
- Kalkofen, W. P. G. S. M. 1994, *Astron. Astrophys.*, 284, 976
- Kwak, H., Chae, J., Song, D., et al. 2016, *Astrophys. J.*, 821, L30, doi: [10.3847/2041-8205/821/2/L30](https://doi.org/10.3847/2041-8205/821/2/L30)
- Lemen, J. R., Title, A. M., Akin, D. J., et al. 2012, *Sol. Phys.*, 275, 17
- Maltby, P., Brynildsen, N., Fredvik, T., Kjeldseth-Moe, O., & Wilhelm, K. 1999, *Sol. Phys.*, 190, 437
- McAteer, R. T. J., Gallagher, P. T., Bloomfield, D. S., et al. 2004, *Astrophys. J.*, 602, 436, doi: [10.1086/380835](https://doi.org/10.1086/380835)
- McAteer, R. T. J., Gallagher, P. T., Williams, D. R., et al. 2003, *Astrophys. J.*, 587, 806, doi: [10.1086/368304](https://doi.org/10.1086/368304)
- Milligan, R. O., Fleck, B., Ireland, J., Fletcher, L., & Dennis, B. R. 2017, *Astrophys. J.*, 848, L8, doi: [10.3847/2041-8213/aa8f3a](https://doi.org/10.3847/2041-8213/aa8f3a)
- Nakariakov, V. M., & Verwichte, E. 2005, *Living Rev. Sol. Phys.*, 2, doi: [10.12942/lrsp-2005-3](https://doi.org/10.12942/lrsp-2005-3)
- Orrall, F. Q. 1966, 917
- OShea, E., Muglach, K., & Fleck, B. 2002, 664, 642, doi: [10.1051/0004-6361](https://doi.org/10.1051/0004-6361)
- Pesnell, W. D., Thompson, B., & Chamberlin, P. 2012, *Sol. Dyn. Obs.*, 9781461436, 1, doi: [10.1007/978-1-4614-3673-7](https://doi.org/10.1007/978-1-4614-3673-7)
- Priest, E. R., & Longcope, D. W. 2017, *Sol. Phys.*, 292, 1, doi: [10.1007/s11207-016-1049-0](https://doi.org/10.1007/s11207-016-1049-0)
- Reznikova, V. E., Shibasaki, K., Sych, R. A., et al. 2012, *Astrophys. J.*, 746, 119, doi: [10.1088/0004-637X/746/2/119](https://doi.org/10.1088/0004-637X/746/2/119)
- Scherrer, P. H., Schou, J., Bush, R. I., et al. 2012, *Sol. Dyn. Obs.*, 9781461436, 207, doi: [10.1007/978-1-4614-3673-7\\_10](https://doi.org/10.1007/978-1-4614-3673-7_10)
- Scheuer, M. A., & Thomas, J. H. 1981, *Sol. Phys.*, 71, 21, doi: [10.1007/BF00153603](https://doi.org/10.1007/BF00153603)
- Schou, J., Scherrer, P. H., Bush, R. I., et al. 2012, *Sol. Dyn. Obs.*, 9781461436, 229, doi: [10.1007/978-1-4614-3673-7\\_11](https://doi.org/10.1007/978-1-4614-3673-7_11)
- Stangalini, M., Del Moro, D., Berrilli, F., & Jefferies, S. M. 2011, 65, 1, doi: [10.1051/0004-6361/201117356](https://doi.org/10.1051/0004-6361/201117356)

- Sutmann, G., Musielak, Z. E., & Ulmschneider, P. 1998, *Astron. Astrophys.*, 340, 556
- Sutmann, G., & Ulmschneider, P. 1995a, *Astron. Astrophys.*, 294, 232
- . 1995b, *Astron. Astrophys.*, 294, 241
- Tian, H., DeLuca, E., Reeves, K. K., et al. 2014, *Astrophys. J.*, 786, 137, doi: [10.1088/0004-637X/786/2/137](https://doi.org/10.1088/0004-637X/786/2/137)
- Viereck, R., Hanser, F., Wise, J., et al. 2007, 66890K, doi: [10.1117/12.734886](https://doi.org/10.1117/12.734886)
- Wittmann, A. 1969, *Sol. Phys.*, 7, 366, doi: [10.1007/BF00146141](https://doi.org/10.1007/BF00146141)
- Woods, M. M., Harra, L. K., Matthews, S. A., et al. 2017, *Sol. Phys.*, 292, doi: [10.1007/s11207-017-1064-9](https://doi.org/10.1007/s11207-017-1064-9)